ELSEVIER

Contents lists available at ScienceDirect

Journal of Colloid and Interface Science

journal homepage: www.elsevier.com/locate/jcis



Light scattering studies of the sol-to-gel transition in particulate systems

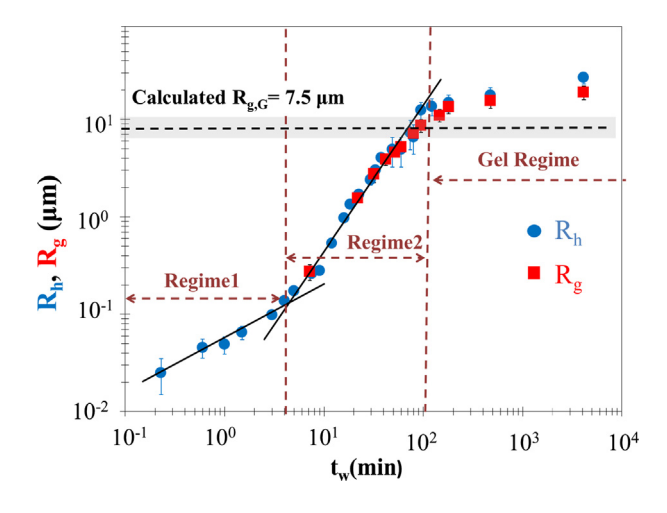


Raiya Husein Ebini, Christopher Michael Sorensen*

Department of Physics, Kansas State University, Manhattan, KS 66506, USA

GRAPHICAL ABSTRACT

The process of sol-to-gel transition involves two kinetics regimes that lead to a gel regime as described by the Ideal Gel Point (IGP) theory.



ARTICLE INFO

Article history: Received 3 June 2019 Revised 19 July 2019 Accepted 20 August 2019 Available online 24 August 2019

Keywords: Aggregation Gelation Light scattering

ABSTRACT

We present investigations of the kinetics of the colloidal sol-to-gel transition by combining small angle static light scattering (SASLS) and dynamic light scattering (DLS) techniques. Dilute monomer volume fractions were used to allow for a full investigation of the gelation to obtain all possible kinetic regimes. Our data verify the predictions of a kinetic theory, the ideal gel point (IGP) theory, where three regimes of kinetics are expected. We observe the first regime, the well-known cluster-dilute regime, with a kinetic exponent of z = 1. Followed by a cluster-dense regime with an enhanced kinetics and z \simeq 2. Finally, a gelation regime is observed where the aggregate growth slows and ceases to grow at the IGP predicted size, $R_{\rm g,G}$. These results quantitatively verify the IGP theory. We conclude that kinetic description provides a complete theory of the gelation process from sol to gel.

© 2019 Elsevier Inc. All rights reserved.

1. Introduction

When colloidal and aero-colloidal dispersions of solid particles aggregate, they form ramified fractal aggregates with a scaling dimension. The scaling dimension is given by the fractal dimension, $D_{\rm f}$ less than the spatial dimension, d. This inequality causes

E-mail address: sor@phys.ksu.edu (C.M. Sorensen).

^{*} Corresponding author at: Department of Physics, Kansas State University in Manhattan, KS 66506, USA.

the mean aggregate size to grow faster than the mean aggregate nearest neighbor distance during aggregation. With this, the aggregate size can overtake the neighbor distance leading to a state in which the entire volume of the dispersion is completely filled by aggregates; this is the colloidal, or aerosol, gel. These gels have physical properties different than the dispersed state. This process is not only fascinating physics, but also such gels are common in nature and are useful to a wide variety of applications [1].

The fractal nature of the aggregates is described by the massradius scaling law:

$$N = k_o (R_g / a)^{D_f} \tag{1}$$

where N is the number of monomers in the aggregate (aggregate's "mass"), $R_{\rm g}$ is the aggregate's radius of gyration, $k_{\rm o}$ is the prefactor, and a is the monomer radius.

Aggregation can be classified into two limiting regimes, diffusion limited and reaction limited cluster-cluster aggregation, DLCA and RLCA, respectively [2]. In DLCA aggregates stick together with high probability when they meet and the resulting fractal dimension of the aggregate is \sim 1.8. In RLCA aggregates stick together with lower probability when they meet, and the resulting fractal dimension of the aggregate in the RLCA can reach up to \sim 2.1 [2]. With the appropriate aggregation kernel, both the DLCA and RLCA regimes are governed by the mean-field Smoluchowski equation (SE) [3,4]:

$$\frac{dn(N)}{dt} = \frac{1}{2} \sum_{i=1}^{i=N-1} K(i, N-i) n(i) n(N-i) - n(N) \sum_{i=1}^{\infty} K(i, N) n(i)$$
 (2)

where n(N) is the number density of aggregates with N monomers in an aggregate, and K(i,j) is the aggregation kernel which controls the rate of the aggregation. Usually K(i,j) is a homogenous function, $K(ci,cj) = c^{\lambda}K(i,j)$, where c is a constant and λ is the degree of homogeneity.

For DLCA the growth kinetics couple the number of monomers per aggregate N to the time via a power law N \sim t^z where z is the kinetic exponent. The SE predicts that the aggregation kernel homogeneity λ , which determines the size distribution [4,5], and the kinetic exponent z, are related by z = 1/(1 $-\lambda$). Thus, the kinetics and the resulting size distribution are linked together [6]. Note that this relationship derives from the SE. For DLCA λ = 0 and z = 1 [7–10].

The SE assumes that the system is cluster-dilute, which means that the mean nearest aggregate neighbor separation $R_{nn}% \left(\mathbf{r}\right) =\mathbf{r}\left(\mathbf{r}\right)$ is much greater than the mean aggregate size $R_{g}\text{, i.e. }R_{nn}\gg R_{g}\text{.}$ these two fundamental length scales grow with different functionalities with N ($R_{\rm g} \sim N^{1/D_f}$ and $R_{nn} \sim N^{1/d}$) causes the system to gel. The gelation process will bring the aggregates relatively close together into the cluster-dense regime where the mean nearest neighbor separation is comparable to the mean aggregate size ($R_{nn} \lesssim 10R_g$). This "cluster-dense" regime can be quantified with the aggregate volume fraction which becomes on the order of 1% when clusterdense. Simulation studies [10] in the cluster-dense regime for the DLCA situation showed that both the effective aggregation kernel homogeneity λ and the kinetic exponent z increase from their cluster dilute limits in a universal fashion with the normalized free volume Ω ; the kinetics speed up. This happens while keeping the relation z = $1/(1 - \lambda)$ satisfied. Ultimately, when the aggregate volume fraction is equal to one, $\lambda = 1/2$ and z = 2. There is a significant experimental literature that supports the description above. Enhanced kinetics have been observed during salt induced aggregation of spherical colloids [11,12] and aqueous suspension of proteins [13]. Enhanced aggregation kinetics were observed in a dense soot aerosol of a heavily sooting flame [14]. Dhaubhadel et al. [15] studied dense aerosol aggregation to find enhanced kinetics and z values as high as 2.3.

The situation, at which the aggregates fill the available volume and "touch", i.e. when the aggregate volume fraction equals unity, is expected to be a special point in the sol-to-gel transition. Although the exact definition of the volume fraction is somewhat arbitrary, to calculate it we have chosen to assume that all the aggregates are the same size, a size given by their perimeter radius, $R_p = [(D_f + 2)/D_f]^{1/2}R_{g_s}$ and they have spherical symmetry. These conditions could vary, but the overall functionalities on R_g and D_f should be good. This definition worked very well in our simulations [16,17]. We shall call the point where this volume fraction equals unity the Ideal Gel Point, IGP. With this definition and based on our previous work, the IGP theory identifies three regimes of aggregation kinetics [16]. Initially, if the monomer volume fraction is small, the destabilized sol (colloid or aerosol) will find $R_{nn} \gg R_g$, the cluster-dilute regime [7-10] with two independent length scales, $R_{\rm g}$ and $R_{\rm nn}$. As aggregation proceeds, $R_{\rm g}$ will grow faster than R_{nn} because $D_f < d$; hence eventually these two length scales will become comparable to each other. Hence they act as one effective length scale and enter the cluster-dense regime [10,15]. Ultimately, with aggregation, the IGP is reached [16]. The condition that the aggregate volume fraction, as described above, equals unity at the IGP leads to the aggregate size at the IGP, R_{g,G}, as:

$$R_{g,G} = a[f_{nm}^{-1}k_o(D_f/(2+D_f))^{3/2}]^{1/(3-D_f)}$$
(3)

where $f_{v,m}$ is the initial monomer volume fraction, which is conserved throughout the aggregation. Wu et al. [12] results validate the $R_{\nu,G}$ dependence on $f_{v,m}$.

Experiments with soot aerosols [15,18–20] and colloids under certain conditions [21] indicate that at the IGP, the resulting aggregate morphology is a hybrid composed of DLCA aggregates with a fractal dimension of 1.8 assembled into a larger superaggregate with a fractal dimension of 2.5. Simulations show that if the constituent DLCA aggregates are treated as supermonomers with mean size R_{g,G}, the superaggregates are isomorphic with clusters formed via the static percolation models with a fractal dimension of 2.5, and these superaggregates appear as a separate phase in the size distribution [22]. Percolation is a static theory hence does not describe the kinetics of the sol-to-gel transition. Nevertheless, recently, it has been shown that percolation is a natural result of kinetic aggregation, thus unifying the kinetic and percolation descriptions of gelation [22,23].

Light scattering is a non-invasive method to probe the kinetics of the sol-to-gel transition. Combining Eq. (1) with N $\,\sim\,\,t^z$ one can find that $R_{\rm g} \, \sim \, t^{z/D_{\rm f}}.$ This will be used to find the z exponent not only in the cluster-dilute regime but also in the cluster-dense regime as the mean field SE holds up to the IGP as shown by Fry et al. [10]. On the other hand, the scattered intensity of an aggregating system I(q) is a function of the scattering wave vector q, where $\mathbf{q} = (4\pi/\lambda)\sin(\theta/2)$. Here λ is the wavelength of the scattered light, and θ is the scattering angle. It can be shown [24] that for any system with no multiple scattering artifacts, the scattered intensity I(q) can be expressed as $I(q) \sim N_c I_c(q)$ where $I_c(q)$ is the scattered light of one cluster and N_{c} is the number of clusters in the system ($N_c = N_m/N$, N_m is the initial number of monomers). At small q values, i.e. $q \sim 0$, $I_c(0) \sim N^2$ [24]. Thus for the entire system $I(0) \sim N_c N^2$. But $N_c N = N_m$ which is conserved throughout the aggregation process, thus $I(0) \sim N$. Combining this with the power law kinetics for DLCA aggregates one gets $I(0) \sim t^z$.

The purpose of this paper is to test experimentally the IGP kinetic theory. Unlike many previous studies of the sol-to-gel transition, we start with a very small monomer volume fraction. This allows not only avoiding the multiple scattering artifacts, but also to start the transition in the cluster-dilute regime and hence fully investigate the broad range of kinetics. We find that the gelation of a dilute ensemble of spherical particles with isotropic attractive

forces evolves through three successive growth regimes to yield a kinetically arrested gel.

2. Experimental methods

The experiments were performed with both non-gelling (aggregating) and gelling systems. Carboxyl modified polystyrene spheres (Molecular Probes) with a diameter of 40 nm, as measured by DLS, were suspended in the buoyancy matching medium of H₂O/D₂O. These particles are electrostatically stabilized by the well-known, Derjaguin-Landau-Verwey-Overbeek (DLVO) potential The electrostatic repulsion and the van der Waals attraction constitute the DLVO potential [25,26]. For stable colloids the electrostatic repulsion creates a barrier in the total potential [27]. Changing the ionic strength of the solution acts to reduces the repulsion barrier [28,29]. If the barrier is reduced to a sufficient level, then the Brownian motion of the particles is capable of overcoming the electrostatic barrier. Then the particles, when in close proximity of each other, can bind together via the van der Waals attraction. In this experiment we choose MgCl₂ (Sigma-Aldrich), a convenient ionic salt, to destabilize the particles. Manely et al. gave an expression to find the gravitational strain value on a cluster [30] and Gisler et al. showed that colloidal aggregate gels break under external strains >0.45 [31]. Following Manely et al., calculations for our system indicate the cluster size at which this critical strain is reached is \sim 80 μ m, which is much higher than the measured size in our experiment.

The non-gelling, aggregating system was very dilute, with a monomer volume fraction $f_{v,m}$ = 6.8×10^{-6} , hence non-gelling for weeks. This system stayed in the cluster-dilute regime during the whole experiment ($\sim\!18$ hrs). Data was collected at different times after the onset of aggregation, a time that will be called the waiting time, t_w . The gelling systems had monomer volume fraction of the order 10^{-4} . For these systems the kinetics was slow enough to allow for detecting all aggregation regimes from the onset of aggregation up to the gel formation within feasible experimental times.

To probe the structure and dynamics we combined small angle static light scattering (SASLS) and dynamic light scattering (DLS) to operate simultaneously. The SASLS set up is similar to that of Ferri [32]. A 512 pixel photodiode array (PDA) (Hamamtsu, model S3902-512) was used for light detection in the SASLS set up. The detectable range of the scattering angle in SASLS was 0.1-14° corresponding to a scattering wave vector q range between ca. $0.03 \ \mu m^{-1}$ to $3.8 \ \mu m^{-1}$. A focused beam of $\lambda = 532 \ nm$ in vacuo (Laserglow, model R533001GX), vertically polarized passed through the sample. For DLS the scattered light was collected via a photomultiplier tube (PMT) (Precision Instruments, model 3262RF) and the signal was correlated using a using a ALV-5000 multiple-tau digital correlator. The PMT was placed on a movable arm to change scattering angle between 22° and 90° alternatively, which corresponds to $q = 6 \mu m^{-1}$ and 22.1 μm^{-1} , respectively. For gel studies both DLS and SASLS were used, whereas for the aggregation experiment (non-gelling) the forward scattering was too weak to be detected by the SASLS detector. DLS yields an apparent radius R_{app}. The results of Lindsay et al. [33] indicate that the apparent radius is the true hydrodynamic radius, R_h , if $qR_h \ll 1$. As $qR_h \rightarrow 1$, rotational diffusion can affect the decay rate of the dynamic correlation function and the apparent radii R_{app} appear smaller than the true R_h . When $qR_h \gg 1$, R_{app} is smaller by a factor of ~2.25. However, we have noticed in the literature some experimental data deviate from this correction for $qR_h \ge 10$. [30,33– 35]. Sandköhler et al. [36] introduced a scattering model that accounts for the contribution to the internal dynamics of fractal clusters. Their model allows to describe the previously measured experimental data and correct for the deviation that was observed for qR_h > 10. We used the Lindsay et al. results for qR_h \leq 10 and the Sandkühler et al. results for qR_h > 10 to obtain the true R_h. For a non-gelling (aggregating) experiment in the cluster-dilute regime, the true hydrodynamic radius R_h, which is obtained from two different scattering angles (22° & 90°) gives experimental z = 0.94 \pm 0.04 hence λ = 0.06 \pm 0.04 when D_f = 1.8 is used. This is in excellent agreement with the values of z = 1 & λ = 0 expected for DLCA in the cluster-dilute regime. Furthermore, the maximum R_h value measured was \sim 10 μ m which is much smaller than the theoretical R_{g,G} \sim 200 μ m calculated using Eq. (2) [16]. Hence this system was indeed non-gelling and remained a suspension of freely diffusing fractal aggregates. For the gelling experiment SASLS and DLS (at 90° scattering angle) were performed simultaneously.

3. Results and discussion

Fig. 1(a) shows the static scattered intensity I(q) vs. q for a gelling sample ($f_{v,m}$ = 3.8 \times 10⁻⁴ and salt concentration [MgCl₂] = 10 mM). The power law slope is evidence of fractal aggregates with a fractal dimension D_f = 1.78 ± 0.05 formed via DLCA. The dynamic field correlation function f(q,t) vs t in Fig. 1(b) shows complete relaxations over all times to indicate that the gelling system remains ergodic. This indicates that the excursions of the seg-

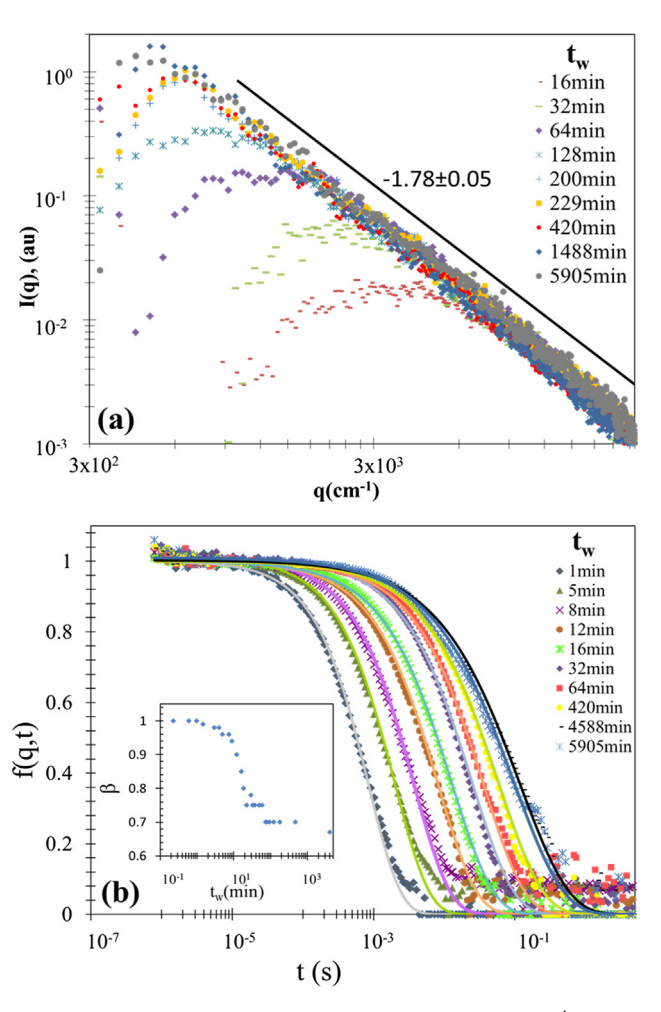


Fig. 1. Light scattering results for the gelling sample $(f_{v,m}=3.8\times10^{-4}~\&~[MgCl_2]=10~mM)$ at various waiting times (t_w) after aggregation initiation. (a) SASLS measured I(q) vs q. The slopes at large q imply $D_f=1.78\pm0.05$. (b) DLS measured dynamic structure factor f(q,t) vs t for the same gelling sample shown in (a). The insert shows the stretching exponent β vs t_w .

ments within the gel is greater than q^{-1} , so the scattering appears ergodic [37]. The solid fit lines in Fig. 1(b) are the fit to a stretched exponential $f(q,t) \sim exp(-t/\tau)^{\beta}$, where τ is the relaxation time and β is the stretching exponent. The insert is a plot β vs. t_w . Initially β takes a value of 1, then drops below that at $t_w \sim 5$ min. The $\beta < 1$ behavior indicates hindered motion of the diffusing aggregates [38,39].

The SASLS provides I(q) vs q graph at different t_w . Each I(q) vs. q provides a measure of the intensity at small q values at that t_w . The hump at smaller q values is due to cluster-cluster anti-correlation [40] which occurs when in the cluster-dense regime [41]. It will be further established below that all the SASLS measurements were taken when the system was in the cluster-dense regime. We will assume that the value of I(q) at the peak of each hump is the value of the intensity at small q. We will call it I(0). SASLS can also be used to find R_g from Guinier analysis. f(q,t) vs. t can be used to find R_h assuming Stokes-Einstein Brownian motion of the aggregates. It is known that $R_h \sim 0.77R_g$ for aggregates in the dilute regime [42]. For the purpose of identifying a general trend of kinetics one may assume $R_h \sim R_g$. Then, each of R_h , R_g , & I(0) can probe the kinetics because $I(0) \sim t^z$ and $R_h \sim R_g \sim t^{z/D_f}$.

Fig. 2 plots R_g , R_h and I(0) versus the waiting time t_w for the gelling colloid with $f_{\nu,m}$ = 3.8×10^{-4} and salt concentration of 10 mM. The three different kinetic regimes are demonstrated. The first regime is immediately after the onset of aggregation and continues up to a time we will call it a transition time $t_{trans}\sim5$ min. After that, there is enhanced aggregation representing the second regime. Finally, the kinetics slows down drastically at the "rounding off time" where $t_w\sim80$ min. R_g , I(0), and R_h vs. t_w graphs obtained from SASLS and DLS were in support of the second and the third regime. The first regime was detected only by the DLS because the aggregate sizes were below the range of the SASLS setup.

The first regime obtained from the R_h vs. t_w plot (Fig. 2) gives a kinetic exponent z = 0.98 \pm 0.07 hence $\lambda \simeq 0$ as expected for a cluster-dilute case [7–10]. At the second regime, which begins at $t_{trans} \sim 5$ min, the data (R_h, R_g and I(0)) indicate a kinetic exponent

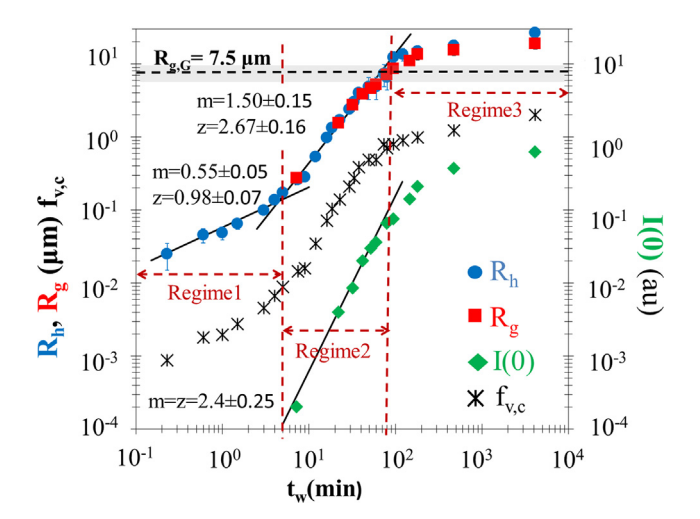


Fig. 2. Temporal evolution of R_h , R_g , I(0), and $f_{v,c}$ for the gelling sample ($f_{v,m} = 3.8 \times 10^{-4}$ and salt concentration [MgCl₂] = 10 mM). R_h vs. t_w shows the three different regimes, R_g and I(0) vs t_w further support the 2nd and 3rd regimes. Solid lines are fits to these symbols and their slopes, m_s , and corresponding dynamic scaling exponents, $z = mD_f$ for R_g or h vs. t_w and m = z for I(0) vs. t_w , respectively. The D_f value used is 1.78 as measured in Fig. 1 (a) and $R_{g,G}$ was calculated using Eq. (2) and marked with black dashed line. The experimental error in D_f gives a range of R_g . G values as indicated by the highlighted area in the graph. The star symbols represent the evolution of the volume fraction of the clusters, $f_{v,c}$, calculated using Eq. (4).

z > 2, as shown on the graph, a value that is higher than the expected z = 2 by the IGP theory. However, a correction of the time scale is appropriate. The correction involves recognizing that the second temporal regime did not start at $t_w = 0$ but rather near the transition time $t_{trans} \sim 5 \text{ min}$ as indicated by the data. When we plot $R_h,\,R_{\rm g}$ & I(0) vs. the $t_w\text{--}t_{trans}$ as indicated by the unfilled symbols in Fig. 3, we find that both radii give an exponent $z = 1.87 \pm 0.14$ to imply $\lambda = 0.47 \pm 0.04$, and I(0) gives $z = 1.80 \pm 0.2$ to imply $\lambda = 0.44 \pm 0.06$. These three measurements are in good agreement with IGP predictions for the cluster-dense regime to have 1 < z < 2 before the IGP is reached. In Figs. 2 and 3 the growth of both R_h and $R_{\rm g}$ starts to drastically slow down and rounds off near the cluster size of $9 \pm 3 \mu m$. The fractal colloidal gels are fragile, such that any gentle shaking can cause the gel to collapse. Thus tests of rigidity or measurement of the shear modulus cannot be used to determine the gel point. Nevertheless. the sol to gel transition is over when the transition ceases, i.e. when temporal evolution of key parameters stops. That is why we define the region of rounding off in the R_g, R_h vs. t_w graph to indicate the time at which the system starts to gel. The cluster size of $9 \pm 3 \mu m$ is in good agreement with the theoretical value of the radius of gyration at the IGP calculated to be $R_{g,G}$ = 7.5 ± 1.8 μ m using Eq. (3) and indicated by the highlighted area. After the rounding off time, R_g and R_h start to take slightly different values. This difference might be due to a couple of factors. One might be due to the correction that was made to the DLC apparent radius in an attempt to obtain the true hydrodynamic radius, R_h as described in the experimental section. Another reason could be the cluster-cluster anti-correlation affecting the R_g SASLS measurement. On top of that, gelation adds to the complexity of the scattering system as the clusters are no longer individual and interdigitation might be taking place.

Computer simulations [10] show that the enhancement of the kinetics is due to the crowding in the cluster-dense regime, where crowding was measured by the normalized cluster free volume Ω . We wish to represent our data in terms of the cluster volume fraction $(f_{v,c})$ which is defined as the ratio of the volume occupied by the clusters to the total volume of the system (V_{sys}) , in other words $f_{v,c} = 1-\Omega$. With the assumption that $R_g \simeq R_h$, the measured R_h value can be used to find the number of monomers per cluster in Eq. (1). Knowing the total number of monomers in the system N_m , the

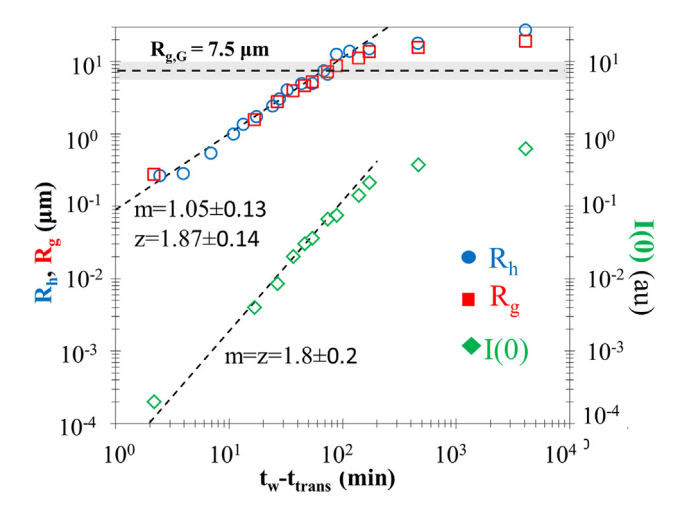


Fig. 3. Temporal evolution of R_g , R_h & I(0) vs. t_w - t_{trans} with their slopes (dashed lines) and corresponding z values. t_{trans} is the time at which cluster-dilute transitions to cluster-dense ($t_{rans} \sim 5$ min in Fig. 2). The D_f used is 1.78 as measured in Fig. 1 (a) and $R_{g,G}$ was calculated using Eq. (2) and marked with dashed line. The experimental error in D_f gives a range of $R_{g,G}$ values as indicated by the highlighted area

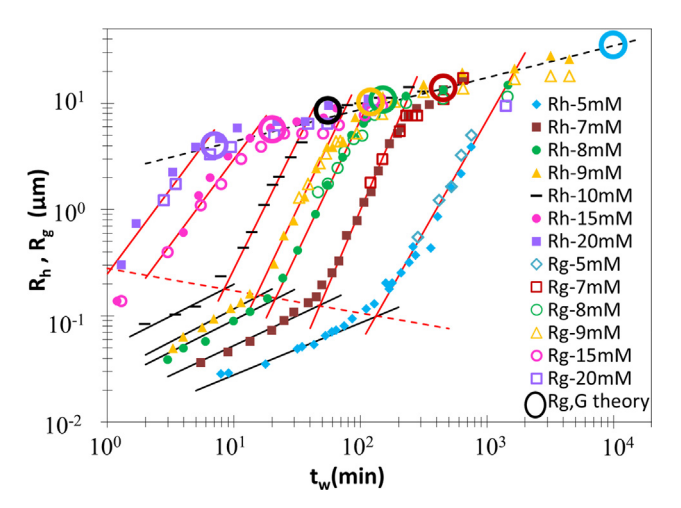


Fig. 4. Temporal evolution of R_h . R_g for the gelling sample $(f_{v,m}=3\times 10^{-4})$ destabilized with different amounts of MgCl₂. R_h vs. t_w shows the three different regimes, R_g vs t_w further supports the 2nd and 3rd regimes. Solid lines are fits to these symbols. The red dashed line is to guide the eye when regime1 transitions to regime2. R_g . was calculated using D_f values, summarized in Table 1, & Eq. (3), then graphed vs t_w at which "rounding off" i.e. IGP occurs as big color coded circles. The black dashed line is used to guide the eye. Summary of the D_f , slopes in regime1 and corresponding z values are found in Table1. (For interpretation of the references to colour in this figure legend, the reader is referred to the web version of this article.)

number of clusters $N_c = N_m/N$ can be found under the assumption of same size, spherical aggregates (the IGP assumptions). To find the $f_{v,c}$ we need to find the total volume of the clusters. Each cluster occupies a volume that is contained within its perimeter. For the assumption of spherically symmetric aggregate one may write the perimeter radius $R_p = [(D_f + 2)/D_f]^{1/2}R_g$. Then the $f_{v,c}$ can be calculated as:

$$f_{\nu,c}(t) = (4\pi/3) [(D_f + 2)D_f]^{3/2} N_c(t) R_g^3(t) / V_{\text{sys}}$$
 (4)

When $f_{v,c}$ vs. t_w is graphed as shown in Fig. 2, the volume fraction of clusters starts to increase from $f_{v,c} = f_{v,m} = 3 \times 10^{-4}$ at $t_w = 0$ to about 1% when the kinetics is transitioning from that expected for cluster-dilute to cluster-dense at t_{trans} . This explicitly demonstrates that crowding enhances aggregation. The third regime is when R_h , R_g , and I(0) are all rounding off showing a drastic slowing down in kinetics. The rounding off indicates the IGP. This rounding correlates well with the $f_{v,c}$ approaching unity. Afterward the $f_{v,c}$ slowly increases above unity to indicate cluster interdigitation.

Fig. 4 shows $R_h \& R_g$ vs t_w for a series of gel experiments with fixed $f_{v,m}$ = 3×10^{-4} but different MgCl₂ salt concentrations (5 mM, 7 mM, 8 mM, 9 mM, 10 mM, 15 mM, and 20 mM). This is in contrast to Fig. 2 which displays a detailed discussion of one experiment. Static scattered intensity I(q) vs. q plots for these concentrations are not shown here, exhibit very similar behavior of Fig. 1(a) except the power law regimes have different slopes for different salt concentrations. The salt concentration and D_f values

are summarized in Table1. The higher values of salt concentrations led to fractal dimensions of 1.73 and 1.8 to imply the DLCA regime. On the other hand, for the smaller salt concentrations the fractal dimensions were larger to imply the diffusion limited regime is giving way to the reaction limited regime. At extreme RLCA, we expect $D_f \sim 2.1$ [2]. Nevertheless, both of these fractal dimensions are significantly different than the spatial dimension, and that difference is the primary reason why the gel is formed.

Fig. 4 displays the growth kinetics for a wide range of MgCl₂ concentrations. The same three regimes of kinetics as demonstrated in Fig. 2 are found. The only exceptions are with the fastest kinetics where cluster-dilute occurred too fast to be detected (the 15 mM and 20 mM cases), and for the slow kinetics where sedimentation occurred before gelation (as the 5 mM case where sedimentation was observed at $t_{\text{w}}\!\sim\!1000\,\text{min})\text{,}$ or probably in a compatible time scale with gelation (as the 7 mM case where sedimentation was observed at $t_w \sim 1300\,\text{min}$). Sedimentation occurred for the 5 mM &7 mM runs due to the cluster size to which the system can grow becoming comparable to the size at which the critical strain is reached (as described in the experimental section). This will affect the z values measured for these two experiments as will be shown below. It is worth mentioning that for the rest of the experiments sedimentation was either never observed or observed at least up to the point tw was more than 10 fold larger than the time where the third regime started, i.e. IGP is reached.

The first regime slopes in Fig. 4 ($m_{regime1}$) and z values ($z_{regime1}$) are summarized in Table1. The experimental z values are slightly higher than, but within uncertainty of, the expected value of 1 for the cluster-dilute regime. Nevertheless, all dilute regimes are followed by the enhanced kinetics of the dense regime which continues up to the rounding off regime where IGP occurs.

Another feature shown in Fig. 4 is the large color coded circles which designate the IGP theory. These large circles were placed in the following manner: at each gel experiment the waiting time at which the third regime the "rounding off" regime occurred is determined from $R_h \ \& \ R_g$ rounding off. This is the time at which gelation starts i.e. the IGP is reached. Then Eq. (3) is used to calculate the theoretical R_g at the IGP i.e. R_{g,G} using the measured D_f values summarized in Table1. The figure shows that the third regime the "rounding off" regime occurred at smaller $R_{\rm g}$ and $R_{\rm h}$ with higher salt concentrations. The higher salt concentration yields smaller D_f; see Table 1. The IGP theory predicts a strong dependence of $R_{g,G}$ on D_f , Eq. (3). The smaller D_f yields smaller $R_{g,G}$ for a fixed f_{v,m} and monomer size. This behavior is mapped very well with the theoretical $R_{g,G}$ values calculated from the IGP theory for each experiment. The black dashed line is used to guide the eye through these points.

To explore the second regime R_h and R_g vs. t_w – t_{trans} must be plotted; hence the transition time t_{trans} for all the experiments must be determined. Fig. 4 shows t_{trans} for all runs except for the 15 mM and 20 mM experiments. To find t_{trans} for these experiments we did the following: from Fig. 4 we observed that the first regime transitions to the second regime in a linear fashion in

Table 1
Summary of the experimental results presented in Fig. 4. The fractal dimension D_6 the slope of regime1 and regime2 ($m_{regime1} \& m_{regime2}$) with their corresponding kinetic exponents values ($z_{regime1} \& z_{regime2}$).

[MgCl ₂] mM	D_{f}	$m_{regime1}$	$Z_{regime1}$	m _{regime2}	Z _{regime2}
5	2.05 ± 0.05	0.5 ± 0.1	1.0 ± 0.2	1.7 ± 0.15	3.5 ± 0.3
7	1.9 ± 0.05	0.56 ± 0.1	1.1 ± 0.2	1.3 ± 0.05	2.5 ± 0.1
8	1.85 ± 0.05	0.6 ± 0.1	1.1 ± 0.2	1.1 ± 0.05	2.0 ± 0.1
9	1.85 ± 0.05	0.62 ± 0.1	1.15 ± 0.2	1.05 ± 0.1	1.9 ± 0.2
10	1.8 ± 0.05	0.6 ± 0.1	1.1 ± 0.3	1.05 ± 0.1	1.9 ± 0.1
15	1.73 ± 0.05			1.0 ± 0.15	1.73 ± 0.3
20	1.73 ± 0.05			1.0 ± 0.2	1.73 ± 0.3

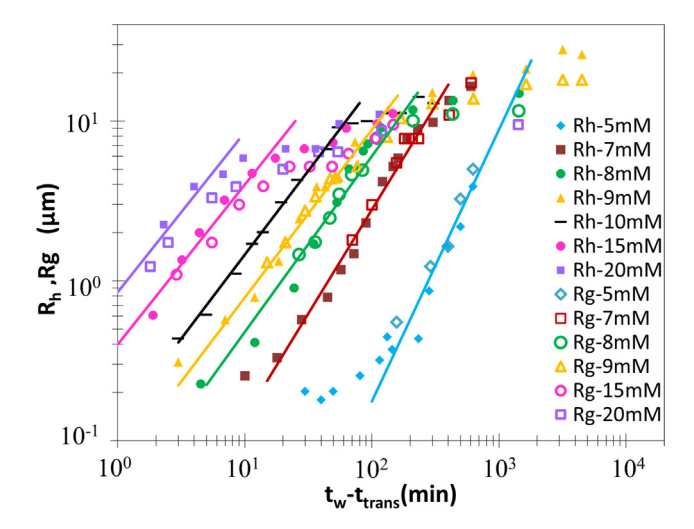


Fig. 5. Temporal evolution of R_h , R_g vs. t_w – t_{trans} for the gelling samples (f_{ν_s} m = 3 \times 10⁻⁴) destabilized with different amounts of MgCl₂. t_{trans} is the time at which the cluster-dilute regime transitions to cluster-dense. t_{trans} values are determined experimentally for each run from Fig. 4. The solid lines are the fits to the data points. Summary of the D_f slopes in regime2 and corresponding z values are found in Table 1.

log-log scale indicated by the dotted red line. By extrapolating this line one can estimate $t_{trans}\sim 2$ min and $\sim \! 1$ min for 15 mM and 20 mM, respectively. Fig. 5 shows R_h and R_g vs $t_w\!-\!t_{trans}$ and slopes for the second regime $(m_{regime2})$ and the corresponding z values $(z_{regime2})$ are summarized in Table 1. The kinetics during the second regime is enhanced i.e. 1 < z < 2 as indicated by the IGP theory for all the experiments except for the 5 mM & 7 mM. As mentioned above, the 5 mM and to less extend the 7 mM experimental z values in the second regime are affected by sedimentation.

An important concept that the IGP theory advocates is the existence of the two fundamental length scales, the average aggregate size, $R_h \sim R_g$, and average mean nearest neighbor separation R_{nn} . These grow with different functionalities with the number of monomers per aggregate, $R_g \sim N^{1/D_f}$ and $R_{nn} \sim N^{1/d}$, which

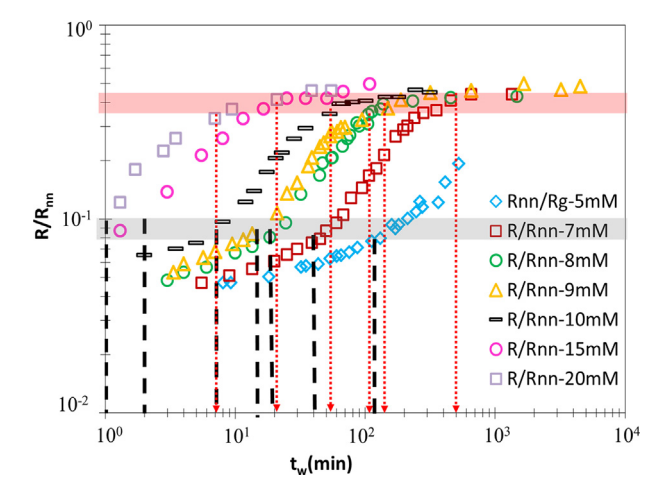


Fig. 6. The temporal evolution of the ratio of the two fundamental length scales in the system; aggregate size divided by the mean nearest neighbor distance, R/R_{nn} vs. t_w . The vertical dashed black lines represent the transition time t_{trans} for each run as determined from Fig. 4. The horizontal grey highlight represents the corresponding range of R/R_{nn} at which t_{trans} occurs for all the runs. The color red pointing down arrows represents the time at which the "rounding off" occurs as determined from Fig. 4 for each run. The red highlight shows the corresponding range of R/R_{nn} at which the "rounding off" i.e. the IGP occurs for all the runs. (For interpretation of the references to colour in this figure legend, the reader is referred to the web version of this article.)

causes the system to gel. To follow the evolution of these two length scales we first define a general size $R \simeq R_h \simeq R_g$. This is reasonable given that our data support the fact that $R_h \simeq R_g$. The mean aggregate nearest neighbor separation is $R_{nn} = (V_{svs}/N_c)^{1/3}$, where $N_c \sim N_m/N$. Fig. 6 compares these two fundamental length scales of the system by plotting the ratio R/R_{nn} vs. t_w. It shows that the clusters grow relatively closer to each other with time. Notice that at the transition time, t_{trans} , $R/R_{nn} \sim 0.08-0.1$ for all the runs, marked by the grey highlight. This is consistent with the reported value based on the IGP theory [16] of $R_{nn} \simeq 10R$ where the system begins the cluster-dense regime. In addition, Fig. 6 shows that the ratio R/R_{nn} stops increasing in the range $\sim\!0.34\text{--}0.43$ when the kinetics slow drastically at the rounding off point (except for 5 mM where sedimentation occurred). This range has been highlighted in red and it is in an excellent agreement with IGP prediction of $R_{nn} \sim 2.3\ R_{\rm g}$ for fractal clusters with D_f = 1.8 to start touching [16]. The question remaining: what is the meaning of the points that occur beyond the IGP? Can these data represent the degree of interdigitation? Recall, in Fig. 2 the cluster volume fraction in the system grows beyond unity at later stages of gelation to indicate interdigitation.

4. Conclusions

The studies that we presented here with low volume fraction colloids allow enough time for the kinetic aspects of the sol-togel transition to be observed in their entirety. We find that the gelation of a dilute ensemble of spherical particles with isotropic attractive forces evolves through three successive growth regimes to yield a kinetically arrested gel. These results are in quantitative agreement with the IGP theory and previous theoretical and simulation studies [11,16–18]. This experiment also unifies gelation in aerosols and colloids through the IGP theory. Here we stress the evolution of the sol to the gel is described by kinetics. In the literature there are other descriptions of gelation: gelation is viewed as a thermodynamic phase transition and a percolation phenomenon.

The thermodynamic description of gelation is based on analogous behavior to phase transitions. For example, in studies of gelling colloids Carpineti et al. [11] observed a peak in the static structure factor S(q) at finite scattering vector q, a distinctive hallmark of spinodal decomposition when a liquid system is quenched from the one phase to two phase regime. Note that such behavior is seen in Fig. 1(a), above. They observed that the temporal evolution of the structure factor at late stages of the colloidal aggregation displayed dynamical scaling, a behavior consistent with a phase transition. However, scaling did not occur during the early stages of aggregation. The kinetics description provides an explanation of these observations. Initially, in the cluster-dilute regime there exists two independent length scales, Rg and Rnn. Given two independent length scales, the structure factor cannot be scaled early in the aggregation; consistent with the observation by Carpineti et al. However, as aggregation proceeds, R_g will grow faster than R_{nn} because D_f < d, and eventually these two length scales approach each other [16]. This is the cluster-dense regime [10,15] with one effective length scale; hence a spinodal-decomposition-like scaling in the structure factor will appear. This is an artifact to the fact that R_{nn} is comparable to R_g [41,43] caused by aggregation kinetics, not thermodynamics.

The thermodynamic description of gelation was strongly supported by Lu et al. who studied a dense colloidal system of particles made attractive via a polymer depletion interaction [44]. The polymer concentration controlled the inter-particle interaction potential range and strength U relative to the thermal energy, U/kT. This ratio, which is thermodynamic in nature, determined when the gelation was initiated, after which an evolving spinodal-

decomposition-like peak in the structure factor appeared. Lu et al. concluded that gelation of spherical particles with isotropic, shortrange attractions is initiated by a thermodynamic instability that triggers gel formation via spinodal decomposition. These observations can be easily explained by the high initial volume fraction of monomers used in the experiment. The aggregating sol finds the cluster-dense and subsequent gel regimes very soon after destabilization, the thermodynamic instability. There is no time to see the two aggregation growth regimes clearly visible in our diluter system; their system simply appears to gel immediately after when the depletion interaction is strengthened. In fact, for any sol, all the thermodynamics really does is initiate the aggregation, after that the whole evolution is kinetic. In light of their work we would conclude that thermodynamics triggers gel formation and gelation boundaries are thermodynamic; but the sol-to-gel mechanism is kinetic.

Percolation theory [45] is another description of the sol-to-gel transition. The evolution of sol to gel is modeled by adding sites or bonds at random to a volume until the connectivity percolates, i.e. a volume spanning cluster appears. Recent simulations from our lab have demonstrated that aggregation kinetics leads to a separate phase of superaggregates with structure isomorphic with percolation clusters [22,46]. Hence in a gelling sol, percolation is a consequence of aggregation kinetics.

In summary, our work leads us to conclude that the sol-to-gel transition (gelation) is a kinetic phenomenon well described by the Ideal Gel Point theory. Thermodynamics can initiate the kinetics when the interparticle interactions are comparable to the thermal energy, kT. The kinetics ultimately leads to a second phase of clusters distinct from the sol, and the clusters in this second phase have a percolated structure.

Declaration of Competing Interest

There are no conflicts to declare.

Acknowledgement

This work was supported in part by NSF Grant AGS 1649783.

References

- C. Jeffrey Brinker, George W. Scherer, Sol Gel Science: The Physics and Chemistry of Sol-Gel Processing, Academic Press, New York, 1990.
- [2] M.Y. Lin, H.M. Lindsay, D.A. Weitz, R.C. Ball, R. Klein, P. Meakin, Nature 339 (1989) 360.
- [3] M. von Smoluchowski, Phys. Z 23 (1916) 585.
- [4] S.K. Friedlander, Smoke, Dust, and Haze: Fundamentals of Aerosol Dynamics, second ed., Oxford University Press, 2000.

- [5] P.G.J. van Dongen, M.H. Ernst, Phys. Rev. Lett. 54 (1985) 1396.
- [6] P. Meakin, Adv. Colloid Interface Sci. 28 (1987) 249.
- [7] R. Jullien, Aggregation and Fractal Aggregates, World Scientific, Singapore, 1987.
- [8] M. Kolb, R. Botet, R. Jullien, Phys. Rev. Lett. 51 (1983) 1123.
- [9] J.E. Martin, D. Adolf, Annu. Rev. Phys. Chem. 42 (1991) 311.
- [10] D. Fry, T. Sintes, A. Chakrabarti, C.M. Sorensen, Phys. Rev. Lett. 89 (2002) 148301.
- [11] M. Carpineti, M. Giglio, Phys. Rev. Lett. 68 (1992) 3327.
- [12] H. Wu, J. Xie, M. Morbidelli, Soft Matter 9 (2013) 4437.
- [13] H. Wu, J. Xie, M. Morbidelli, Biomacromolecules 6 (2005) 3189.
- [14] C.M. Sorensen, W.B. Hageman, T.J. Rush, H. Huang, C. Oh, Phys. Rev. Lett. 80 (1998) 1782.
- [15] R. Dhaubhadel, F. Pierce, A. Chakrabarti, C.M. Sorensen, Phys. Rev. E 73 (2006) 011404.
- [16] C. Sorensen, A. Chakrabarti, Soft Matter 7 (2011) 2284.
- [17] D. Fry, A. Chakrabarti, W. Kim, C. Sorensen, Phys. Rev. E 69 (2004).
- [18] C.M. Sorensen, W. Kim, D. Fry, D. Shi, A. Chakrabarti, Langmuir 19 (2003) 7560.
- [19] W. Kim, C.M. Sorensen, D. Fry, A. Chakrabarti, J. Aerosol Sci. 37 (2006) 386.
- [20] W. Kim, C.M. Sorensen, A. Chakrabarti, Langmuir 20 (2004) 3969.
- [21] T. Mokhtari, A. Chakrabarti, C.M. Sorensen, C. Cheng, D. Vigil, J. Colloid Interface Sci. 327 (2008) 216.
- [22] W.R. Heinson, A. Chakrabarti, C.M. Sorensen, Phys. Rev. E 95 (2017) 052109.
- [23] P. Liu, W.R. Heinson, C.M. Sorensen, R.K. Chakrabarty, J. Colloid Interface Sci. 550 (2019) 57.
- [24] C.M. Sorensen, Aerosol. Sci. Technol. 35 (2001) 648.
- [25] B.V. Derjaguin, L. Landau, Prog. Surf. Sci. 43 (1941) 30.
- [26] E.J.W. Verwey, J.T.G. Overbeek, K. Van Nes, Theory of the Stability of Lyophobic Colloids: The Interaction of Sol Particles Having an Electric Double Layer, Elsevier Publishing Company, 1948.
- [27] J.C. Berg, An Introduction to Interfaces & Colloids: The Bridge to Nanoscience, World Scientific, 2010.
- [28] L. Ehrl, Z. Jia, H. Wu, M. Lattuada, M. Soos, M. Morbidelli, Langmuir 25 (2009) 2696.
- [29] Z. Jia, C. Gauer, H. Wu, M. Morbidelli, A. Chittofrati, M. Apostolo, J. Colloid Interface Sci. 302 (2006) 187.
- [30] S. Manley, L. Cipelletti, V. Trappe, A. Bailey, R.J. Christianson, U. Gasser, V. Prasad, P. Segre, M. Doherty, S. Sankaran, Phys. Rev. Lett. 93 (2004) 108302.
- [31] T. Gisler, R.C. Ball, D.A. Weitz, Phys. Rev. Lett. 82 (1999) 1064.
- [32] F. Ferri, Rev. Sci. Instrum. 68 (1997) 2265.
- [33] H.M. Lindsay, R. Klein, D.A. Weitz, M.Y. Lin, P. Meakin, Phys. Rev. A 38 (1988) 2614.
- [34] M.Y. Lin, H.M. Lindsay, D.A. Weitz, R.C. Ball, R. Klein, P. Meakin, in: Proc. R Soc. Lond. A, The Royal Society, 1989, pp. 71–87.
- [35] M.Y. Lin, H.M. Lindsay, D.A. Weitz, R. Klein, R.C. Ball, P. Meakin, J. Phys. Condens. Matter 2 (1990) 3093.
- [36] P. Sandkühler, M. Lattuada, H. Wu, J. Sefcik, M. Morbidelli, Adv. Colloid Interface Sci. 113 (2005) 65.
- [37] A. Krall, D. Weitz, Phys. Rev. Lett. 80 (1998) 778.
- [38] S.Z. Ren, W.F. Shi, W.B. Zhang, C.M. Sorensen, Phys. Rev. A 45 (1992) 2416.
- [39] R. Böhmer, Phase Transit. Multinatl. J. 65 (1998) 211.
- [40] C. Oh, C.M. Sorensen, J. Nanoparticle Res. 1 (1999) 369.
- [41] H. Huang, C. Oh, C.M. Sorensen, Phys. Rev. E 57 (1998) 875.
- [42] C.M. Sorensen, Aerosol. Sci. Technol. 45 (2011) 765.
- [43] J.J. Cerdà, T. Sintes, C.M. Sorensen, A. Chakrabarti, Phys. Rev. E Stat. Nonlin. Soft Matter Phys. 70 (2004) 051405.
- [44] P.J. Lu, E. Zaccarelli, F. Ćiulla, A.B. Schofield, F. Sciortino, D.A. Weitz, Nature 453 (2008) 499.
- [45] D. Stauffer, Introduction to Percolation Theory, Taylor and Francis, London, 1985.
- [46] P. Liu, W. R. Heinson, C. M. Sorensen, R. K. Chakrabarty, (2018).